RSC Advances

This is an *Accepted Manuscript*, which has been through the Royal Society of Chemistry peer review process and has been accepted for publication.

Accepted Manuscripts are published online shortly after acceptance, before technical editing, formatting and proof reading. Using this free service, authors can make their results available to the community, in citable form, before we publish the edited article. This *Accepted Manuscript* will be replaced by the edited, formatted and paginated article as soon as this is available.

You can find more information about *Accepted Manuscripts* in the Information for Authors.

Please note that technical editing may introduce minor changes to the text and/or graphics, which may alter content. The journal's standard Terms & Conditions and the Ethical guidelines still apply. In no event shall the Royal Society of Chemistry be held responsible for any errors or omissions in this *Accepted Manuscript* or any consequences arising from the use of any information it contains.

ROYAL SOCIETY OF CHEMISTRY

www.rsc.org/advances

Crystallographic, optical and dielectric properties of gel grown Praseodymium malonate single crystals.

Nazir Ahmad[1], *M .M. Ahmad*[1], *P. N. Kotru**[2]

[1]Condensed Matter Physics Laboratory, Department of Physics, National Institute of Technology, Hazratbal Srinagar - 190006, Jammu and Kashmir, India.

[2] Crystal Growth and Materials Research Laboratory, Department of Physics and Electronics, University of Jammu, Jammu-180006- India.

Abstract

Single crystals of Praseodymium malonate hexahydrate are grown by gel encapsulation technique. Single and powder X-ray diffraction data so obtained on these crystals is analysed and the internal structure and molecular configuration are worked out. The analysis of crystallographic data shows that the compound crystallises in monoclinic crystal system with space group P2/m. The compound adopts extended 3-D framework stabilized by extensive hydrogen bonding. High resolution X-ray diffraction results suggest that the crystals grown are of good quality. The optical characteristics as obtained from UV-Vis-NIR spectral data are described. The direct forbidden energy band gap is calculated to be 5.4 eV. Results of photoluminescence, refractive index and birefringence measurements are described and discussed. It is shown that the material has a low value dielectric constant and so can be a promising material for microelectronic device applications. The dependence of dielectric constant, dielectric loss and conductivity on frequency of the applied ac field is described and discussed. The results are correlated with those of optical and high resolution X-ray diffraction.

Keywords: Molecular structure; XRD; HRXRD; Optical properties; Dielectric characteristics.

***Corresponding author**: P. N. Kotru.

Present address: Crystal Growth and Materials Research Laboratory, Department of Physics and Electronics University of Jammu, Jammu-180006- India. Fax: 0194-2420475.

Email: pnkotruphy@gmail.com; Tel: +9101912453079, +919419181690.

RSC Advances Accepted Manuscript

1. Introduction

Malonates of rare earth elements are an interesting and fascinating subject of research in material science. Malonates are salts of malonic acid; the latter being the next higher homologue of oxalic acid. Malonate ligand exhibits a flexible stoichemistry and variable mode of binding with metal ions in the crystalline state [1-4]. Non-radiative intra-molecular energy transfer process occurs in those materials which consist of co-ordination compounds of rare earth ions usually trivalent (Pr^{3+}) with organic ligands (malonic acid). Due to antenna effect these materials have potential applications in new technologies such as efficient phosphors, fluorescence, photosensitive bio-inorganic compounds, high technology optics and a fundamental step for high emission quantum yield.

To the author's best knowledge, there is no report till date regarding perfection, optical and dielectric characteristics of praseodymium malonate single crystals. The crystallographic data published in the literature [5-7] earlier is different from the one reported here. The reliability index factor R in the data presented here being far more accurate.

2. Experimental

Chemicals used in the present investigation include, Praseodymium chloride Hexahydrate (99.99%) of Chengdu Haoxuan Technology Co. Ltd. China,

RSC Advances Accepted Manuscript

Sodium meta silicate (99.50%) from Thomas Baker, Mumbai, India and L-Tartratic Acid (99.0%) from Loba-Chemie Indoaustranal Co., Mumbai, India. The crystallisation apparatus used for the growth of single crystals of praseodymium malonate hexahydrate (hereafter called as PMH) by silica gel method involves the use of borosilicate glass tube of length 20cm and inner diameter 2.5cm as crystalliser. The gel solution consisting of sodium mata silicate and malonic acid and adjusted to a particular pH value was then transferred to several crystallisers. It would take around 24 hours for the gel to set in summer (35-40 ^{0}C) whereas in winter (temperature in the range of around 10-20 ^{0}C), it would take a couple of weeks depending upon the pH value and molarity of sodium meta silicate gel. After the gel got set an aqueous solution of $PrCl_3$ of the desired molarity was gently poured along the sides of the crystalliser so as to avoid any gel breakage. In order to conduct experiments to study effect of surrounding temperature on the growth of crystals, the tubes were placed in a thermostatically controlled water bath, wherein the surrounding temperature was maintained constant for each experiment ranging from 30-60 ^{0}C. Temperature > 40 ^{0}C led to liesegang ring formation and poor quality of crystals. The diffusion of Pr^{3+} ions through the narrow pores of the silica gel (gel matrix) leads to reaction between these ions present in the upper reactant (UR) and $(C_3H_2O_4)^{2-}$ ions present in the gel as lower reactant (LR). The following reaction results into crystallisation of Pr malonate crystals.

RSC Advances Accepted Manuscript

$$2PrCl_3 + 3CH_2(COOH)_2 \longrightarrow Pr_2(C_3H_2O_4)_3 + 6HCl.$$

Morphology of the grown crystals was studied using optical and scanning electron microscopy (SEM, Model JEOL 840). The energy dispersive spectrometer (OXFORD ISIS-300 system) attached to the SEM was used to analyze the stoichiometry of the grown crystals. Carbon, hydrogen contents in the grown crystals were determined using Vario EL III CHNS analyzer. Powder X-ray diffraction pattern was recorded using Bruker AXS D8 advanced powder diffractometer with Cu K_α radiation (α = 1.5406 Å) at a scanning rate of 2^0/min with 2θ in the range 10^0- 50^0. Single crystal X-ray diffraction was carried out using single crystal Oxford X-ray diffractometer. The data so obtained was analyzed with SHEL X. To assess the crystalline perfection of the grown crystals, a PANalytical X'Pert PRO MRD HRXRD using Cu Kα radiation and developed at National Physical Laboratory, New Delhi was used. The rocking curve of the crystal for (110) diffraction planes was recorded in symmetrical Bragg geometry using the (110) natural faces by performing ω scan keeping detector of 2theta fixed during ω scan. The highly monochromatic X-ray beam (Cu Kα_1) incident on the specimen was obtained using the four-bounce Ge(220) monochromator. The diffracted beam from the specimen was detected using a scintillation detector with a triple-axis three-bounce Ge(220) analyser. Varian Cary 5000 spectrophotometer was used for optical characterization in the wavelength range of 25-2485 nm from which absorption measurements were

RSC Advances Accepted Manuscript

carried out. Crystals of thickness 1.33 mm were used for the said study. Single crystals of same thickness were used for the Photoluminescence spectroscopy emission spectra using a Perkin Elmer LS-55 luminescence spectrometer in the wavelength range 400-560 nm at room temperature. The area of the crystal surface exposed to the incident beam was kept constant. A cut-off filter of 390 nm was used to separate out the excitation wavelength from the emission spectra reaching the photomultiplier tube (detector). Refractive index studies were carried out using Brewster's angle method. The crystals of 1.33 mm thickness were used for these studies using Abbe refractometer 2WA. Birefringence was conducted by using Exicor –DUV refractometer. In order to ensure good ohmic contact between the opposite (110) faces of a single crystal for investigation into the dielectric behaviour, the crystal was coated with high grade silver paste, ensuring that the paste does not spread along the sides of the crystal. The capacitance and the dissipation factor of the parallel plate capacitor formed between a pair of electrodes having the sample of PMH as a dielectric medium was measured. The measurements were recorded with the help of precision LCR meter model Agilient-4284A and further automated by using a computer for the data recording, storage and analysis. Room temperature dielectric behavior of the sample was recorded on application of ac field (in the frequency range 20Hz-1MHz), using Agilent 4285A precision LCR meter.

3. Results and discussion

RSC Advances Accepted Manuscript

3.1. Single crystal growth and stoichiometric analysis

The optimum conditions determined from a series of experiments leading to single crystals are established to be gel conc. 0.5M, LR conc. 0.5M, UR conc. 0.25, gel age 140 hours, gel pH 6 and temperature in the range of 35-40 ^{0}C; the maximum size of crystals under these optimum conditions being 17mm ×2.5mm ×1.5mm. The mode of growth is dendritic under all the conditions of growth. The tips of these dendrites develop into good quality single crystals of good morphology as they grow deeper into the gel, as shown in fig. 1. The UR concentration greater than 0.75M and LR concentration above 0.5M, leads to spherulitic crystal growth. Liesegang ring formation takes place at higher concentrations > 0.75M of UR as shown in fig. 2. In fact, the spherulitic growth seems to get predominant if one moves deeper into the gel column. The Liesegang rings nearer to the gel reactant interface are a combination of crystals with spherulitic morphology alongwith small tiny single crystals. The crystals of PMH grown under optimum conditions are quite transparent with developed natural faces as shown in fig. 3. Fig. 4 is a scanning electron micrograph of a single crystal of PMH illustrating smooth and flat (110) habit faces of the crystal. The morphological development of the grown crystal is shown in a schematic diagram of fig. 5.

RSC Advances Accepted Manuscript

The experimental and theoretical results of EDAX and CH analysis are compiled in tables 1(a) and 1(b) respectively which suggest the stoichiometric composition to be $[Pr_2 (C_3H_2O_4)_3 (H_2O)_6]$.

3.2. X-ray diffraction

Powder X-ray diffraction pattern of PMH is shown in fig. 6.The diffraction pattern depicts the crystallinity of the grown crystal. CRYSFER and powder-X software were used for analysing the data. Single crystal XRD of the crystal was also recorded. The grown crystals belong to monoclinic system with space group P2/m. Taking (hkl) parameters as obtained from the powder XRD, the crystal may be said to fall in unit pyramid sub-system which is also analogous with sub-system of the unit prism of the monoclinic prism system. The lattice parameters for the crystal turn out to be; a= 15.107 Å, b=11.976 Å and c = 10.343 Å; $\alpha= \gamma=90^0$ and $\beta= 121.508^0$. The volume of the unit cell V = 1871.2704 $Å^3$. The cell parameters worked out here turn out to be different from what is reported in the literature [5-7] which is because of the absolute difference in the internal bonding of the compound as is confirmed from the crystallographic data obtained from the single crystal XRD. Interplanar spacing (d) values were calculated with the help of lattice parameters which are in good agreement with the experimental (d) values. Various parameters like (hkl), interplaner spacing (d in Å), full width half maxima of the diffraction peaks (FWHM) and crystallite size (L in Å), micro strain (ε), dislocation density ρ (ρ

RSC Advances Accepted Manuscript

in 10^{15} m/m^3) and distortion parameter (g) were calculated by using the following well known equations which are recorded in tables 2(a) and 2(b).

$L= K/\beta\cos\theta$; $d=\lambda/2\sin\theta$; $\varepsilon= \beta\cos\theta/4$; $\rho= 1/L^2$ and $g= \beta/\tan\theta$, where $\lambda= 1.54$Å is the wave length of the Cu-Kα X-ray radiation used, β is the full width half maxima (FWHM) of the diffraction peaks, θ is the Braggs angle (in degrees) and K is Scherer's constant (usually taken as 0.89).

Single crystal X-ray diffraction studies were carried out on a single crystal of dimensions 0.35 x 0.30 x 0.25 mm^3. Data was collected at 296(2) K using graphite monochromatic Mo K_α radiation by using oscillation method. The data was interpreted and refined by SHEL X to work out the internal structural details. Based on this data, molecular configuration and molecular packing were worked out. Figs. 7 (a) and (b) show ORTEP diagrams and fig. 8 depicts packing diagram of the molecule when viewed along *c*-crystallographic direction. The interesting feature of this compound is that, two Pr ions are co-ordinated with three ligands and six molecules of water. The bonding behavior of the two Pr ions in the complex is so symmetrical that CIF file of the compound is unable to distinguish one Pr ion with respect the second one; that is why in the ORTEP diagram of the compound, Pr is symbolized as Pr_1 at both the places. This is also one of the distinguishable factors and has a significant impact on bonding of the compound, which in other words modifies all the structure sensitive properties of the material accordingly and differentiates this

RSC Advances Accepted Manuscript

compound from the one reported in the literature [5-7]. Symmetry in the compound leads it towards a sharp melting point.

The crystallographic analysis of [Pr_2 $(C_3H_2O_4)_3(H_2O)_6$] shows that structure consists of three- dimensional metal-organic framework. The Pr is coordinated to six oxygen atoms of four carboxylate groups of different malonate anions. The Pr is additionally coordinated to three oxygen atoms of a water molecule generating a nine-coordinated tricapped trigonal prism constituted by OW(5), OW(6), OW(8), O(1), O(3), O(4), O(7) and O(9). There are two crystallographically independent dicarboxalate malonate anions in compound [Mal. (1) and Mal.(2)] corresponding to O(3)O(4)C(3) and O(1) O(2)C(1)C(5), O(8)O(9)C(5) set of atoms respectively shown in scheme 1.

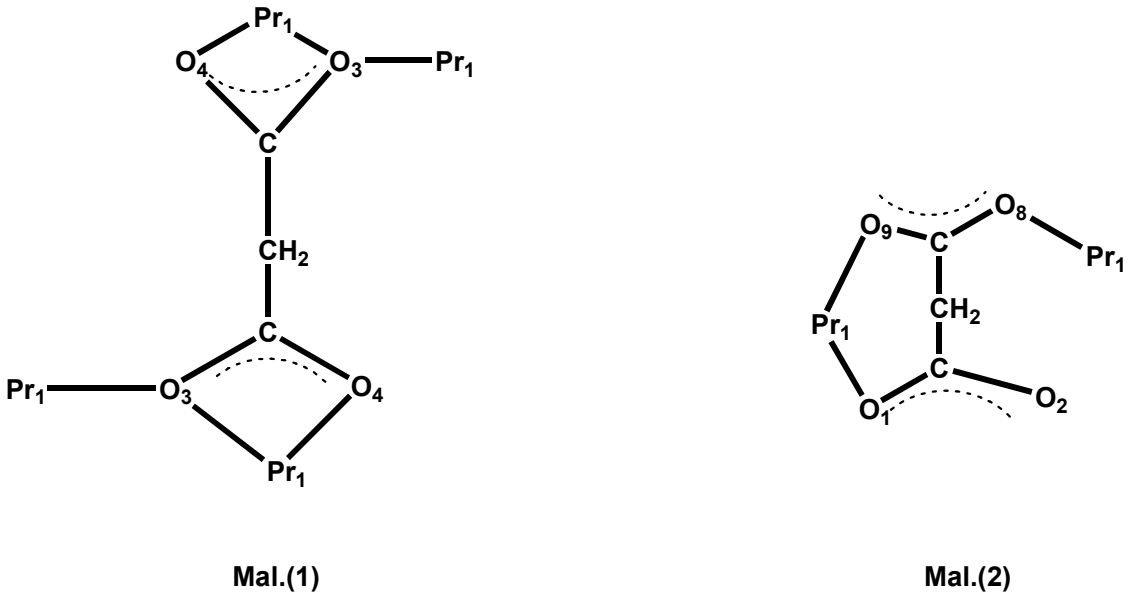

Mal.(1) Mal.(2)

Scheme 1. Co-ordination modes of Mal. 2^- in [Pr_2 $(C_3H_2O_4)_3(H_2O)_6$].

RSC Advances Accepted Manuscript

Mal. (1) adopts the μ_4-$\kappa^2 OO'$; $\kappa O'$;$\kappa^2 O''O'''$;$\kappa O'''$ coordination mode bidendate through O(3) and O(4) toward Pr and monodendate across O(3) towards another Pr and the atoms symmetry related. Mal. (II) act as bidendate through O(1) and O(9) towards Pr and bridging monodendate through O(8) μ_2-κO;$\kappa O'$;$\kappa O''$. The molecule adopts extended 3-D framework when viewed along *c*-crystallographic orientation. The compound is packed in such a fashion that Pr ions act as nodes alternatively while different malonate anions bridge the adjacent Pr ions. One bridging carboxylate group O(4)C(3)O(3) of malonate anion cross links the linear chains as indicated in respective ORTEP and packing diagrams. The distance between the two Pr metal ions is 11.615(8) Å which is different from the reported values [5-7]. The bond length between Pr and oxygen of water molecule is 2.57 Å. Each Pr ion is coordinated with three water molecules and these water molecules stabilize the extensive three dimensional frameworks through extensive hydrogen bonding. The molecule has both intra and intermolecular hydrogen bonds of the type O—H----O. In all the hydrogen bonds O(3) O(4) O(5) and O(6) of water molecules act as both donors and accepters whereas carboxylate oxygen O(3) O(4) O(1) O(9) O(2)… act as acceptors.

For the sake of clarity comparison of single crystal XRD data pertaining to this compound as reported in the literature [5-7] and the present paper are similar in terms of stoichiometric composition, extensive framework of hydrogen bonds

RSC Advances Accepted Manuscript

which stabilizes the entire structure and co-ordination number. However, it differs from the reported ones in terms of space group, cell parameters, cell volume, reliability index factor R, internal molecular features like metal ion distances and symmetrical bonding nature of metal ion with the ligands.

3.3. High-resolution X-ray diffraction

Fig. 9 shows HRXRD rocking curve for (110) diffraction planes of PMH. One finds single and sharp peak with FWHM 19 arc sec which is indicative of good crystal quality free from structural grain boundaries. However, it is interesting to note that there is asymmetry in the rocking curve. As we can see for a fixed angular deviation (θ) of glancing angle with respect to the peak position, the scattering intensity is maximum in the positive direction in comparison to that of the negative direction indicating that the crystal contains more of interstitial type of defects than vacancy defects. Due to interstitial defects (impurities or self-interstitials at interstitial sites), the lattice around these defects undergo compressive stress [8] resulting into decrease in interplanar spacing (d). As a consequence of this it leads to more scattering intensity which is sometimes also known as diffuse X-ray scattering at slightly higher Bragg angles (θ_B) (d and $\sin\theta_B$ being inversely proportional to each other in the well- known Bragg's equation). The reverse is true if it were a vacancy defect [9]. It is worth noting that there are no multiple peaks in the rocking curve which suggests that the

RSC Advances Accepted Manuscript

density of interstitial defects is low and so does not affect the long range order of the crystal [10].

3.4. Optical characteristics

Fig. 10 is a UV-Vis-NIR spectrum recorded on the crystal. It shows the absorption peaks at 272, 443, 475, 595, 1020, 1442, 1552, 1609, 1994 and 2482 nm. In order to determine the nature of transitions and value of the optical band gap, the optical absorption coefficient α was calculated using the relation: α = 2.303×A/t, where t is the thickness (1.33 mm) of the single crystal. According to the Tauc relation [11] the absorption coefficient (α) for a material is given by the relation: $(\alpha h\upsilon) = A(h\upsilon - Eg)^p$, where E_g is the optical band gap, h the Plank's constant, υ the frequency of incident photons and 'p' is the index that characterizes the optical absorption process; p is theoretically equal to 2, 3, 1/2 and 3/2 corresponding to indirect allowed, indirect forbidden, direct allowed and direct forbidden transitions respectively [12, 13]. The plot of $(\alpha h\upsilon)^{3/2}$ versus $h\upsilon$ is shown in fig.11. The band gap was estimated by taking $h\upsilon$ in the high absorption range followed by extrapolating the linear portion to zero abscissa giving the band gap [14]. The direct forbidden energy band gap estimated to be 5.4 eV is found to be the prominent transition that takes place in the material and the value so obtained is in close proximity of other tartrate and malonate based single crystals [15].

RSC Advances Accepted Manuscript

It is clear from the spectrum that there are number of absorption peaks with different areas of cross section throughout the entire spectrum. Absorption peak at 272 nm corresponds to C=O in which $n \rightarrow \pi^*$ transition occurs. Absorption peaks at 443, 475 and 595 nm are very sharp peaks with decimal absorption coefficients and are due to forbidden $f \rightarrow f$ transitions which may appear because of the point defects (interstitial sites); normally defects in crystal structure generally act as photon trapping centers and absorb light radiation leading to poor transparency (absorbance) as the same is clear from the rocking curve of the HRXRD shown in fig. 9. From 625-960 nm there is a wide transmittance window (less absorbance), which is a good sign for PMH in connection with its use in multi- electronic industry [16, 17]. Absorption bands occurring at 1020, 1442, 1552, 1609, 1994 and 2482 nm are highly diffused and are due to vibrational modes of the molecule. It is worth mentioning here that the ordinate axis of fig. 10 shows the less absorption coefficient. This reflects that they are highly transparent in nature as energy is absorbed by the ligand and the same is transmitted by the metal. This property enhances the applications of lanthanides (Pr^{3+}) co-ordinated with organic ligands (malonic acid) which are used as fluorescent materials in the industry.

Rare earth materials are not good absorbers due to forbidden *4f–4f* inner transitions. However, by 'antenna effect' as proposed by Lehn, these materials

RSC Advances Accepted Manuscript

when co-ordinated with organic ligands could be seen as light conversion molecular devices.

Fig. 12 shows the Photoluminescence (PL) emission of PMH. It follows the down -conversion process, because in Ln containing materials, the *4f* transitions are strictly forbidden because of parity reasons. In case of Pr^{3+} there are as many as 327 levels of 4*f* configuration. These levels further increase in number due to crystal field splitting and when these rare earth ions are coordinated with a ligand, more and more splitting takes place. As such they are not directly good absorbers. However, such a behaviour can be developed by co-ordinating rare earth ion (Pr^{3+}) with organic ligands (malonic acid). Generally, down-conversion is a phenomenon whereby one or more photons of higher energy are absorbed by a material and re-emitted as a lower energy photon. Materials able to cause this effect are known as down-converters. In the present PL experiment the material has been tuned (excited) over a wide range of wavelength from 200 to 850 nm, so as to get a good absorption peak. The wavelength of 272 nm was found to be feasible for excitation and the corresponding intense peak was found to be at 445 nm. The crystal shows strong blue emission. Presences of point defects generally act as photon trapping centers [18] and absorb light radiation which is responsible for the blue emission by the material. The HRXRD results support the presence of point defects [19]. Since in organic ligands, organic chromophores are good absorbs than Ln ions, the ligand to

RSC Advances Accepted Manuscript

metal energy transfer is most probable due to antenna effect which helps to increase the luminescence efficiency of Pr^{3+} ions.

The refractive index studies were conducted using Brewster's angle method on single crystal of 1.33 mm thickness. The crystal was mounted on a rotating mount at an angle varying from 0 to 90 degrees. Following the principle of polarization, the crystal was rotated till the reflection of the laser beam disappeared. This angle was noted and Brewster's angle (θ_p) was measured to be 57.3^0. The refractive index was calculated using the relation $\mu = \tan\theta_p$, which turns out to be 1.56.

Birefringence measurements were also undertaken on PMH single crystals of 1.33mm thickness. The light from He-Ne laser source was allowed to pass through optical plane of the crystal, when placed in between the polarizer and the analyzer. The transmitted light from the analyzer that undergoes interference forms the fringe pattern which appears on the screen. The crystal was rotated to capture the interference pattern which appeared to be distorted. The distorted nature in fringes could be due to various types of defects present in the crystal, like strain during growth, point defects, color centers or any other [20]. The HRXRD studies show that the crystals do contain point defects. Due to presence of defects, the intensity of emergent light from the crystal got diminished. To calculate the birefringence ($\Delta\mu$), following relation was used [21]

$$\Delta\mu = \lambda/\pi t \sin^{-1}(I/I_0)^{1/2}$$

RSC Advances Accepted Manuscript

Where I and I_0 are the intensity of light before and after passing through the crystal and t is the crystal thickness. Position of the sample was continuously varied till maximum intensity of light came out and the value of $\Delta\mu$ was determined to be 0.01593 which is in good proximity with other semi-organic crystals [21, 22]. This study helps us to locate exactly the optic axis and the growth orientation along the same axis of the grown crystal.

3.5. Dielectric behaviour

Single crystal with prominent (110) faces was mounted between a pair of electrodes. The dielectric constant ε_r was computed using the relation:

$\varepsilon_r = 4Ct/0.0885A$

Where C represents the capacitance of the crystal, t the thickness and A the area of the crystal. Single crystals with a very low dielectric constant value are required by industries dealing with microelectronic technology [23]. L- arginine oxalate and L-arginine acetate are also reported to be low value dielectric materials [23]. It is worth to mention that the dielectric characteristics reported here for PMH single crystal identify it to be a promising material having potential application in microelectronics. The dependence of dielectric constant (ε_r) and dielectric loss ($\tan\delta$) on frequency of the applied ac field in case of PMH is studied within the frequency range of 20 Hz to 1MHz. Dielectric characteristics are supported by the optical properties and HXRD results of the

RSC Advances Accepted Manuscript

crystal. The variation of ε_r with frequency is as shown in fig. 13. It is clear that there is a resonance peak at a very low frequency and the dielectric constant of the material is quite high in this region. The dielectric constant starts to decrease with further increase in frequency of the applied ac field. Such type of behaviour is a normal trend of the dielectric materials. The gradual decrease in dielectric constant with frequency suggests that the material under consideration has ferroelectric domains of different sizes and hence varying relaxation times [24]. In the low frequency range all the types of polarisation mechanisms (electronic, ionic, dipolar and space charge) may be active [25-27]. As the frequency increases, a point will be reached where the space charge cannot sustain and comply with the external field [28]. Space charge polarisation is responsible for high value of dielectric constant at lower frequencies, which indicates the lesser number of defects in the crystal. Such a situation is more important for optical applications [29]. This observation supports the crystalline perfection of the grown crystal, as also revealed from the high resolution XRD rocking curve of the crystal for (110) diffraction planes described earlier.

The variation of dielectric loss (tanδ) with frequency is shown in fig.14. The figure reveals that the dielectric loss is high at lower frequency and decreases with increase in frequency. At higher frequency all the polarisation mechanisms are not operative and the energy need not be spent on rotating the dipoles. As a result dielectric loss is also minimum. The characteristic of low dielectric loss

RSC Advances Accepted Manuscript

with high frequency for the sample suggests that the crystal possesses enhanced optical quality with lesser defects and this parameter plays a vital role for the construction of devices from nonlinear optical materials [30, 31].

The ac conductivity $\ln\sigma_{ac}$ is calculated by substituting the value of (capacitance given directly by the instrument) in the formula $\sigma_{ac} = 2\pi f\varepsilon_0\varepsilon_r\tan\delta$; where ε_0 stands for the absolute permittivity in the free space having value of 8.854×10^{-12}F/m and f is the frequency in hertz. Fig. 15 shows the variation of conductivity with frequency. In order to study the nature of the conductivity as a function of frequency, Jonscher's power law as given below has been used [32,33]:

$$\sigma(\omega) = \sigma_0 + A\omega^s$$

Where ω is angular frequency, σ_0 is frequency independent factor (DC conductivity) and s is a power exponent which is a function of temperature and can be calculated by plotting $\log\sigma$ versus $\log\omega$. The value of s lies within the limits $0 \leq s \leq 1$ [34]. When s=0, the electric conduction is frequency independent (dc conduction) which refers to conductivity at very low frequency. When $s > 0$, the conduction is frequency dependent which means ac conduction [64]. In the present study, s was calculated from the plot of $\log\sigma$ versus $\log\omega$ as shown in fig. 16 at ambient temperature which comes out to be s=0.011. This value of 's' suggests that the electrical conductivity for this crystal is determined by the hopping conduction of proton transport within the frame-

RSC Advances Accepted Manuscript

work of hydrogen bonds due to presence of water molecules. Detailed thermo-analytical studies of the material have been conducted which confirm the presence of six water molecules in the present material and the details of the same will be communicated elsewhere. In the present case, the conductivity increases smoothly with increase in frequency. As such there is no sharp increase that would be the characteristic of a superprotonic phase transition [25]. Pycnometric density and x-ray density of the title compound do not differ which goes in support of our observation that there exists some fraction of point defects in the crystal. That goes in support of the variation of conductivity of the type reported here [35]. Here, we can conclude that the increase in conductivity in PMH is due to the presence of hydrogen bonds. It is reported [24] that the conduction in tartrates and malonates are due to rotation of tartrate/malonate ions. There is a finite probability that when the temperature of the tartrate/malonate crystal approaches 300K, the bonds of the hydrogen gets weakened due to the rotation of tartrate/malonate ions and they give rise to L and D-defects. This results in an enhanced conduction in these materials [24]. Other possibility is the presence of point defects which also plays essential role in the conduction process. The optical and HRXRD results confirm the same.

4. Conclusion:

Gel technique of crystal growth yields single crystals of PMH with prominent (110) habit faces; the stoichiometric composition is established to be

RSC Advances Accepted Manuscript

$[Pr_2(C_3H_2O_4)_3(H_2O)_6]$. The optimum conditions of growth are gel conc. 0.5M, LR conc. 0.5M, UR conc. 0.25, gel age 140 hours, gel pH 6 and temperature in the range of 35-40 ^{0}C. HRXRD suggests that the crystals grown under the optimum conditions are of good quality. The crystal falls under monoclinic system with lattice having space group P2/m and cell parameters as a= 15.107 Å, b=11.976 Å and c = 10.343 Å; $\alpha = \gamma = 90^0$ and $\beta = 121.508^0$ and V = 1871.2704 Å^3. Based on the single crystal XRD results, the molecular arrangement within the internal structure is worked out. The crystallographic data presented here differentiates it from the one reported in the literature in respect of reliability factor, space group, cell parameters and molecular arrangement. UV-Vis-NIR spectrum indicates optical absorption peaks at 272, 443, 475, 595, 1120, 1442, 1552, 1609, 1954, 2482 nm of wavelength. The forbidden energy band gap is estimated at 5.4eV. Photoluminescence study leads to down-conversion process taking place in the compound. Refractive index measurements of the crystal lead to a value 1.55. The birefringence $\Delta\mu$ of the crystal is calculated to be 0.01593. The crystal of PMH is shown to have a low dielectric constant and can thus be a promising material for the microelectronic device applications.

Acknowledgments:

The author (Nazir Ahmad) is highly thankful to Prof. Rajat Gupta, the Director, NIT Srinagar and Prof. Fayaz Ahmad Mir, Registrar NIT Srinagar, for taking keen interest and extending financial support for carrying out this research

RSC Advances Accepted Manuscript

work. The author is thankful to Dr. K. K. Maurya, Scientist at NPL, New Delhi for HRXRD facilities and Prof. H. N. Sheikh, Department of Chemistry, University of Jammu, for useful discussions. The author is also thankful to Mr. P. L. Saproo of NIT, Srinagar for his generous help and understanding.

References

[1] K. Matsumoto, H. Kuroya, Bull. Chem. Soc. Jpn. 45 (1972) 1755

[2] N.J. Ray, B.J. Hathaway, Acta Crystallogr., Sect. B 38 (1982) 770;

[3] R. Hamalainen, A. Pajumen, Suom. Kemistil., B 46 (1973) 285;

[4] Anastas Karipides, James Ault, A. Thomas Reed, Inorg. Chem. 16 (1997) 3299.

[5] B. H. Doreswamy, M. Mahendra, M.A. Sridhar, J.S. Prasad, P.A. Varughese, K.V. Saban, G. Varghese, J. Mol. Struct. 659 (2003) 81-88.

[6] M.H. Molina, P.A.L. Luis, T. Lopez, C.R. Perez, F. Lloret, M. Julve, Cryst. Eng.Comm.31 (2000) 1-5.

[7] E. Konstantina, Chrysomallidou, P. Spyros, Perlepes, A. Terzis, C.P. Raptopoulou, Polyhedron, 29 (2010) 3118–3124

[8] G. Bhagavannarayana, S. Parthiban, S. Meenakshisundaram, Cryst. Growth Des. 8 (2008) 446-451.

RSC Advances Accepted Manuscript

[9] S.K. Kushwaha, K.K. Maurya, N. Vijayan, G. Bhagavannarayana, Cryst. Eng. Comm. 13 (2011) 4866-4872.

[10] G. Bhagavannarayana, S.K. Kushwaha, M. Shakir, , K.K. Maurya, J. Appl. Crystallogr. 44 (2011) 122-128.

[11] J. Tauc, Amorphous and Liquid Semiconductors, Plenum, NewYork, (1974) 159-220.

[12] V. Krishnakumar, D.K. Awasti, Fouran Singh, P.K. Kulriya, R. Nagalaskshmi, Nuc. Instrum. Methods Phys. Res. B 256 (2007) 675.

[13] S.K. Arora, V. Patel, B. Chudasama, B. Amin, J. Cryst. Growth 275 (2005) 657.

[14] R. P. Khatri, S. M. Vyas, P.J. Patel, D. Shah, M.P. jani, Asian, J. Chem. 21 (2000) 135.

[15] P.P. Kumar, V. Manivannan, P. Sagayaraj, J. Madhavan, Bull. Mater. Sci. 32 (2009) 431.

[16] P.N.S. Kumaria, S. Kalainathan, characterisation of lead (II) Chloride single crystals grown in silica gel. Cryst. Res. Technol, 43 (2008) 413-416.

[17] D. Kalaisevi, R.M. Kumar, R. Jayavel, Single crystal growth and properties of semiorganic nonlinear optical L-arginine hydrochloride monohydrate crystals. Cryst. Res. Technol. 43 (2008) 851-856.

RSC Advances Accepted Manuscript

[18] H. Xu, D. Lee, S. B. Sinnott, V. Gopalan, V. Dierolf, S. R. Phillpot, Phys. Rev. B, 80 (2009) 144104.

[19] S. J. Xu, G. Li, S. J. Chua, X. C. Wang, W. Wang, Appl. Phys. Lett. 72 (1998) 2451-2453.

[20] V. Vasudevan, R.R. Babu, A.R. Nelcy, G. Bhagavannarayana, K. Ramamurthi, Bull. Mater. Sci 34 (2011) 469-475.

[21] A.M. Nasr, Int. J. Mater. Sci. 2 (2007) 103.

[22] Y. Zhang, H. Li, B. Xi, Y. Che, J. Zheng, J. Mater. Chem. Phy. 108 (2008) 192.

[23] M. Meena, C.K. Mahadevan. Mater.Lett.;62 (2008) 3742–3744.

[24] Nazir Ahmad, M.M. Ahmad, P.N. Kotru; J. Cryst. Growth 412 (2014) 72-79.

[25] M. Meena, C.K. Mahadevan, Cryst. Res. Technol. 43 (2008) 166–172.

[26] S.M. DharmaPrakash, P.M. Rao, J. Mater. Sci. Lett. 8 (1989) 1167

[27] N. Vijayan, G. Bhagavannarayana, G.C. Budakoti, B. Kumar, V. Upadhyaya, S. Das, Mater. Lett. 62 (2008) 1252.

[28] S. Kuryan, R. Abraham, J. Isac; Indian J. Pure Appl. Phys., 46 (2008) 30.

RSC Advances Accepted Manuscript

[29] A.C. Peter, M. Vimalan, P. Sagayaraj, J. Madhavan; Arch. Appl. Sci. Res., 2 (2010) 191.

[30] S.A. Martin Britto Dhas, S. Natarajan; Opt. Commun., 281 (2008) 457.

[31] D. Kalaiselvi, R.M. Kumar, R. Jayavel; Cryst. Res. Technol., 43 (2008) 851.

[32] A.K. Jonscher, The universal dielectric response; Nature 267 (1977) 673-679.

[33] A.K. Jonscher, A new understanding of the dielectric relaxation of solids; J. Mater. Sci., 16 (1981) 2060.

[34] M.D. Ingram, Ionic conductivity in glass, Phys. Chem Glasses; 28 (1987) 215-234.

[35] C.C. Desai, A.N. Hanchinal; J. Mat. Sci. Lett. 4 (1985) 419-421.

RSC Advances Accepted Manuscript

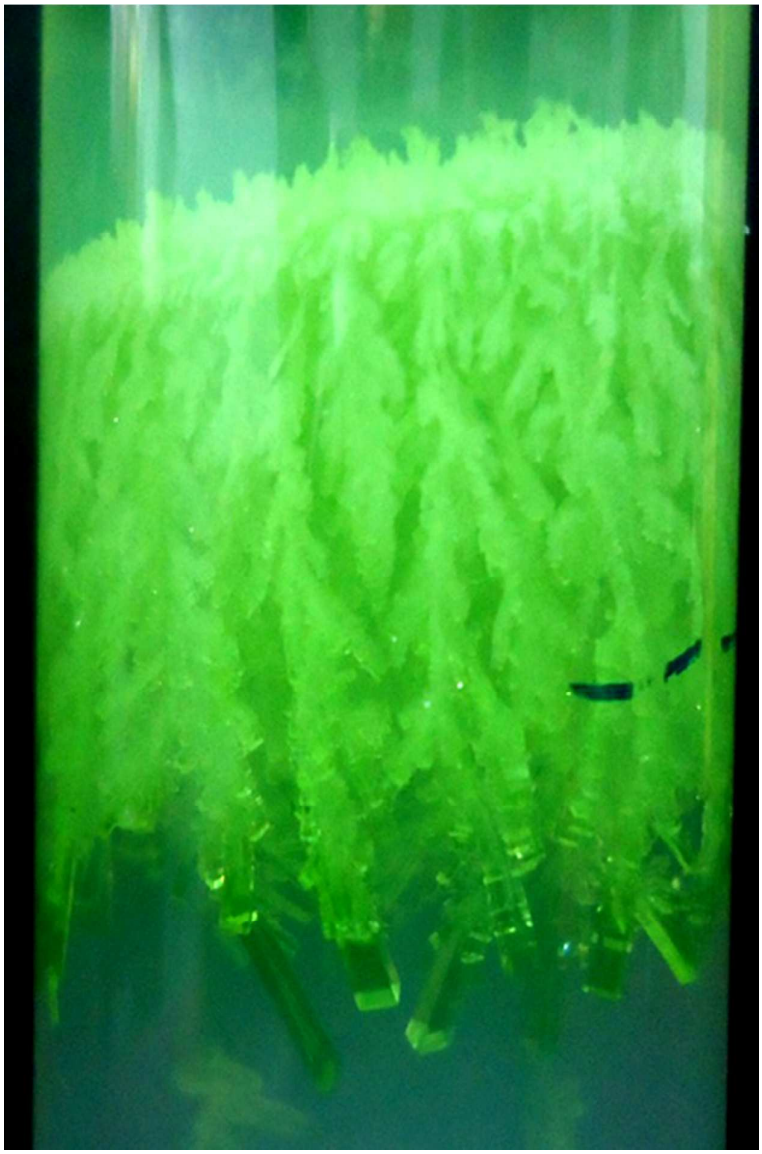

Fig.1. Single crystals of PMH developing from the tips of the dendritic formation in the gel.

RSC Advances Accepted Manuscript

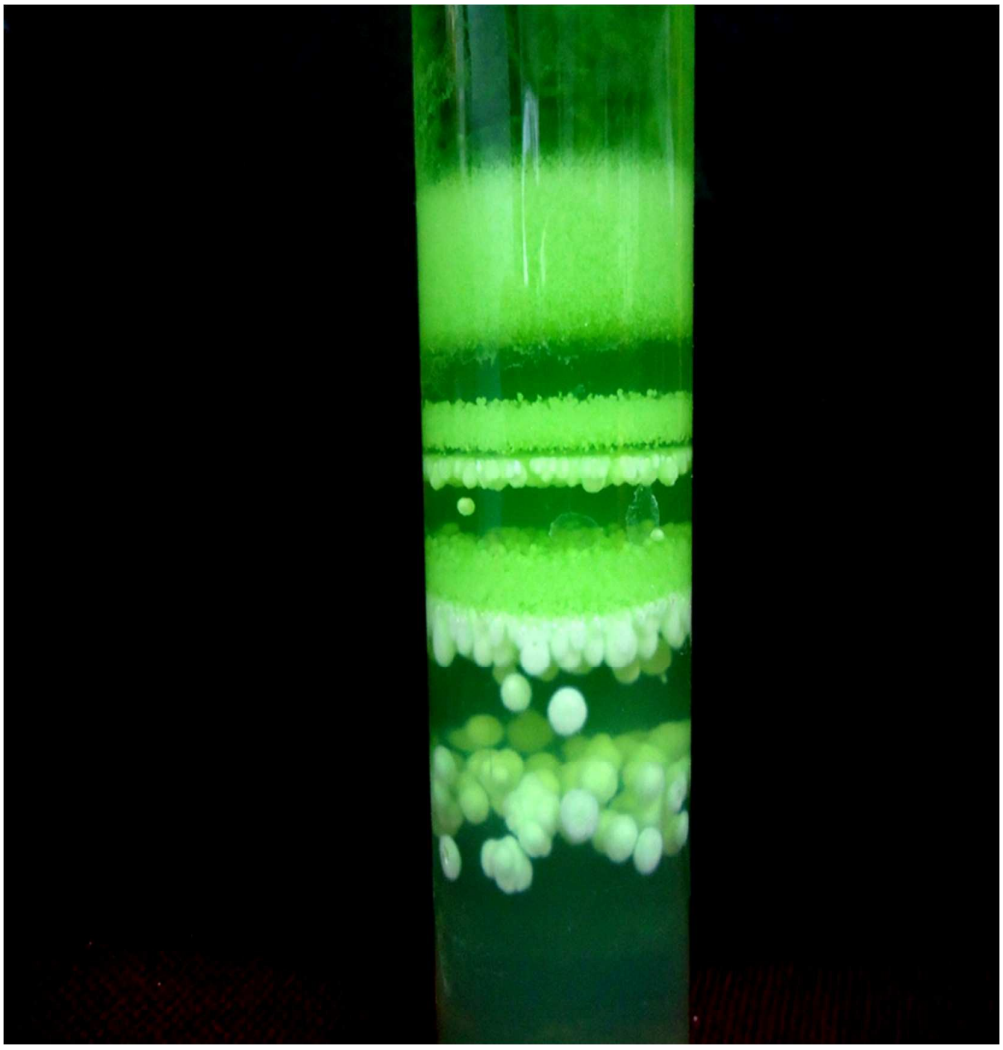

Fig.2. Liesegang ring formation in the crystallizer with U.R conc. > 0.75M.

RSC Advances Accepted Manuscript

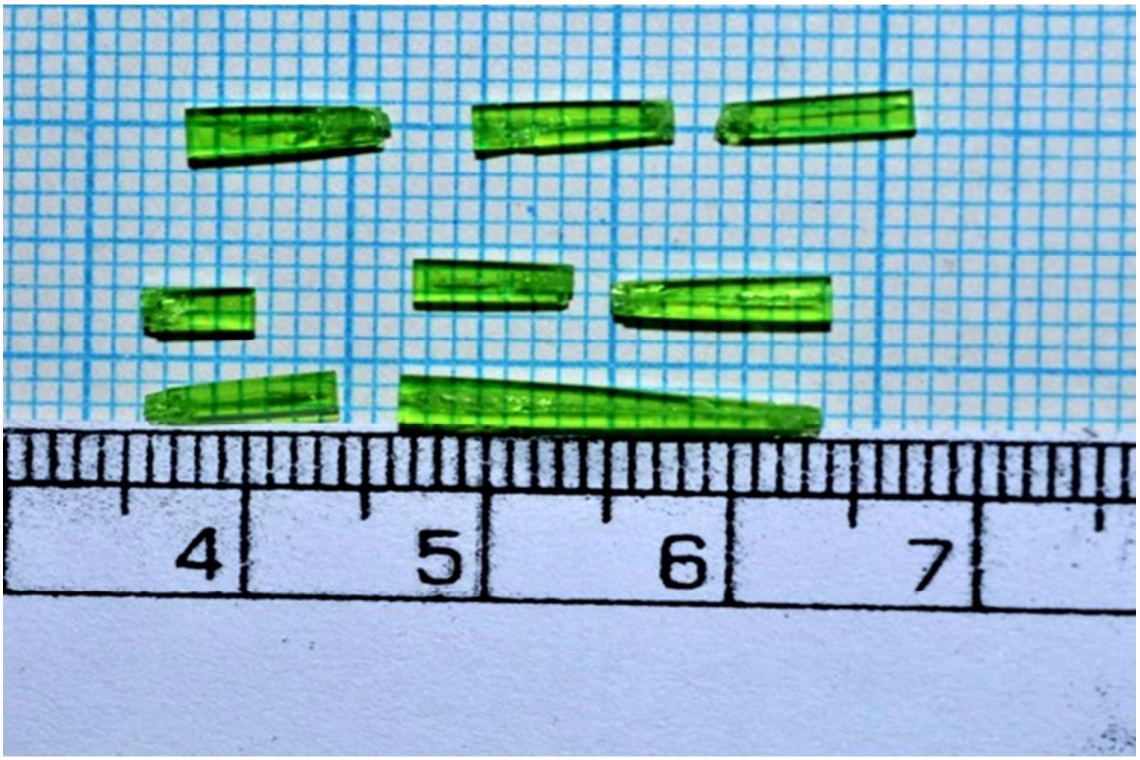

Fig.3. Single crystals of PMH grown under optimum conditions of growth.

RSC Advances Accepted Manuscript

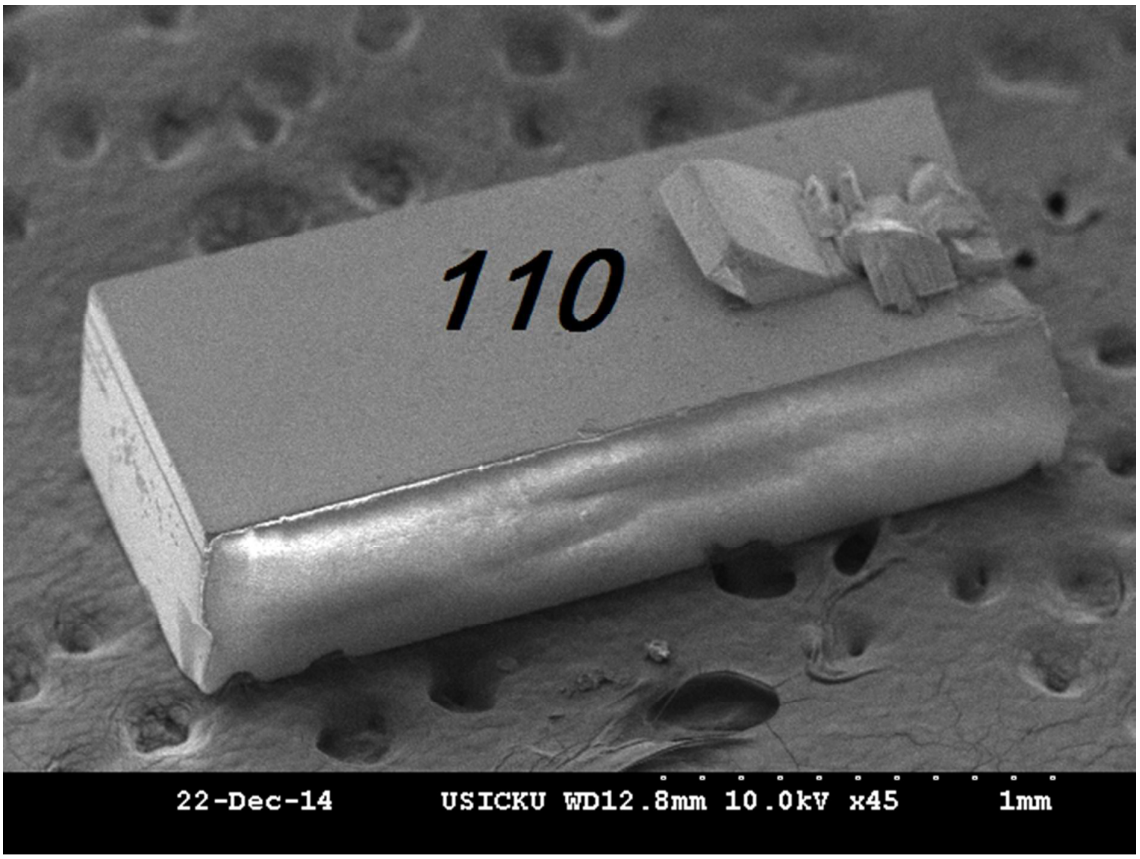

Fig.4. SEM of PMH as grown under optimum conditions of growth revealing its morphology.

RSC Advances Accepted Manuscript

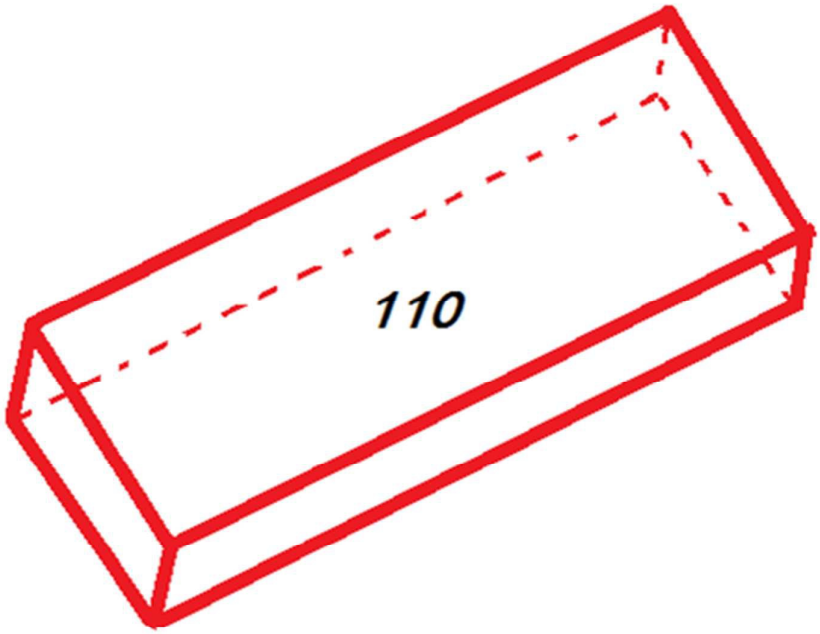

Fig.5. Schematic diagram illustrating the morphology of the grown crystal with prominent (110) habit faces.

RSC Advances Accepted Manuscript

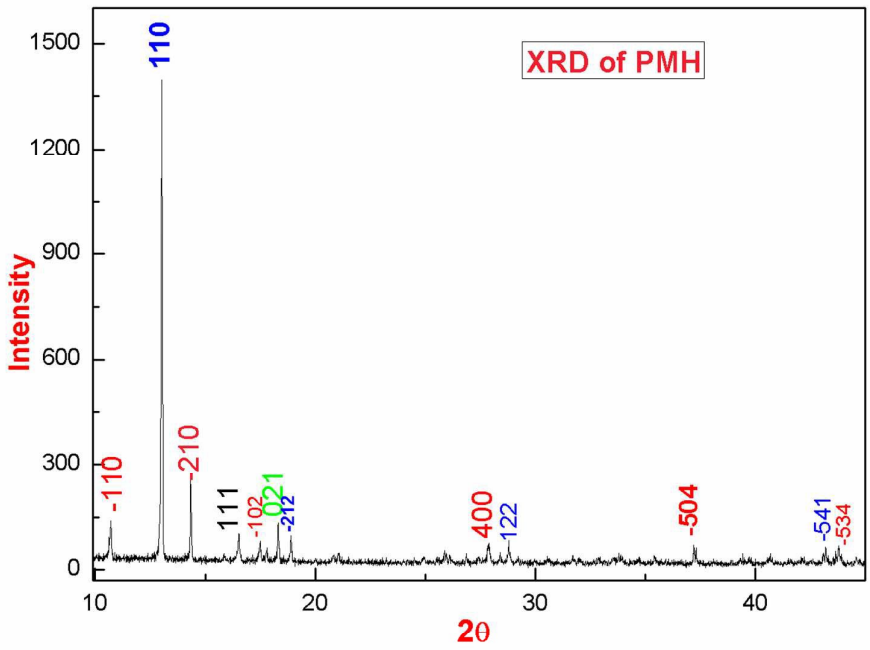

Fig.6. Powder X-ray diffraction Pattern of PMH showing (110) peak as the dominant one.

RSC Advances Accepted Manuscript

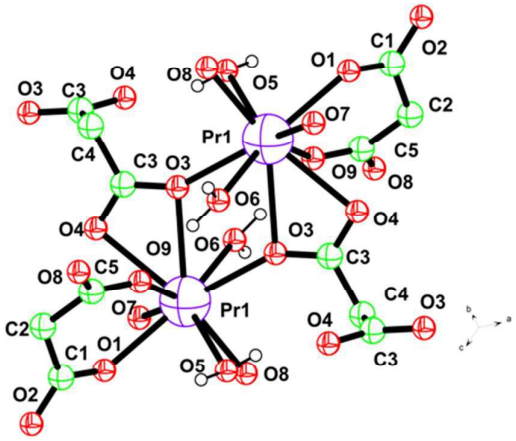

Fig. 7 (a). ORTEP diagram of [Pr_2 $(C_3H_2O_4)_3(H2O)_6$] single crystal.

RSC Advances Accepted Manuscript

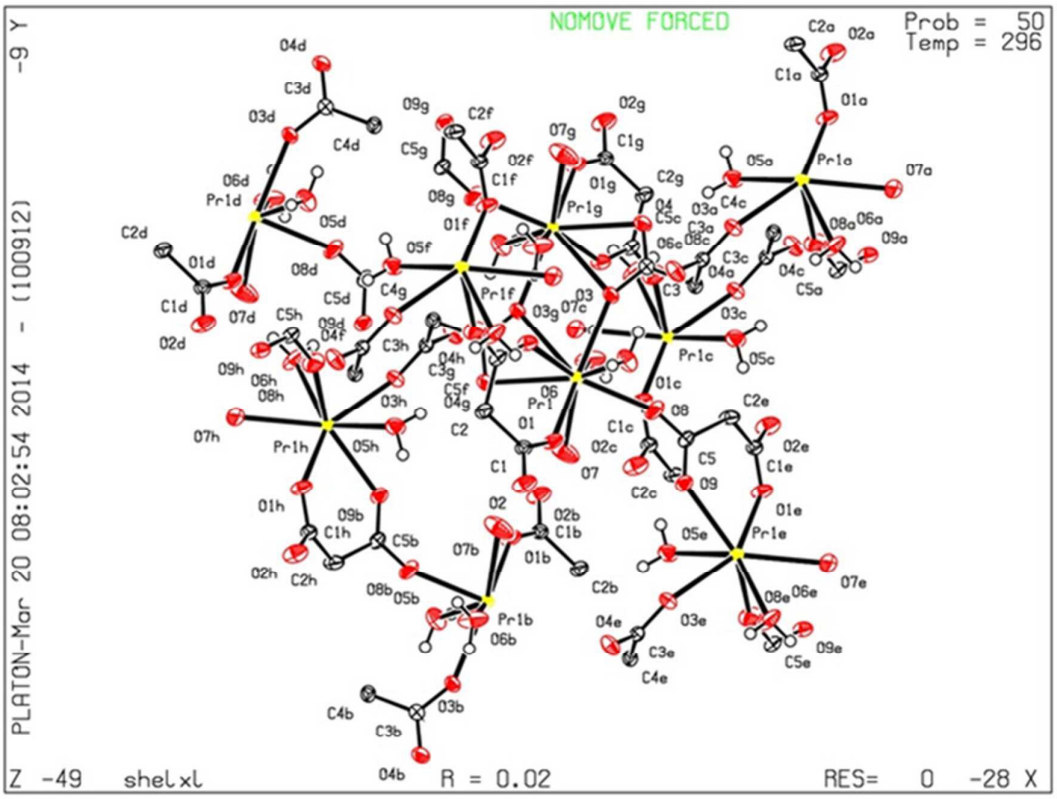

Fig. 7 (b). ORTEP diagram of $[Pr_2(C_3H_2O_4)_3(H_2O)_6]$ single crystal (full structure).

RSC Advances Accepted Manuscript

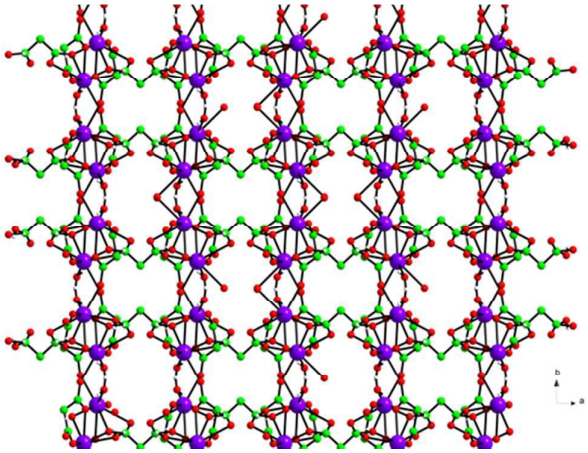

Fig.8. Packing diagram of [Pr_2 $(C_3H_2O_4)_3(H_2O)_6$] single crystal.

RSC Advances Accepted Manuscript

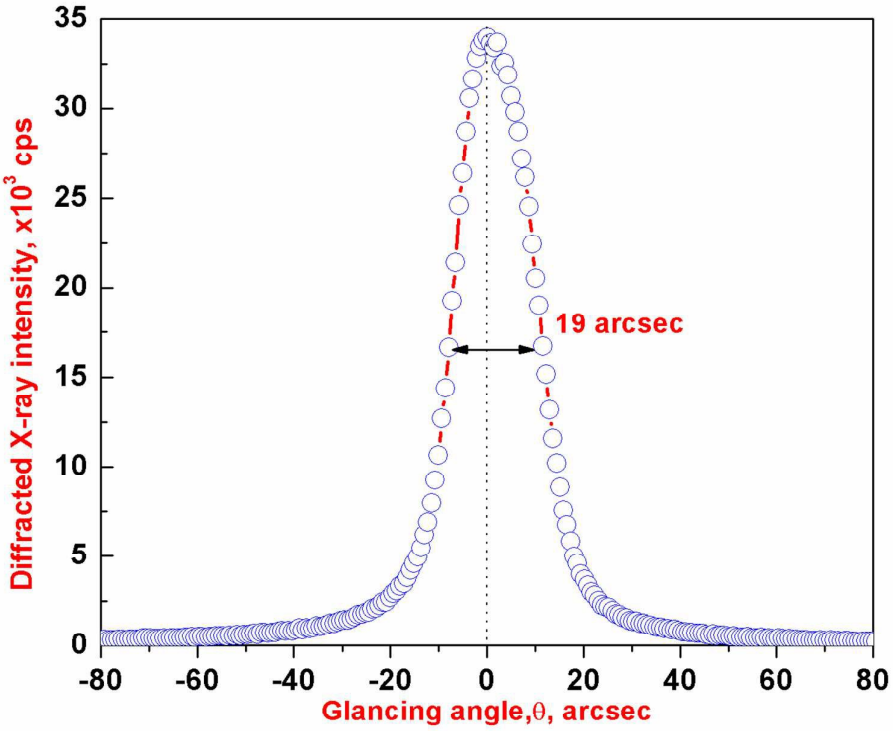

Fig. 9. HRXRD of (110) plane of PMH single crystal.

RSC Advances Accepted Manuscript

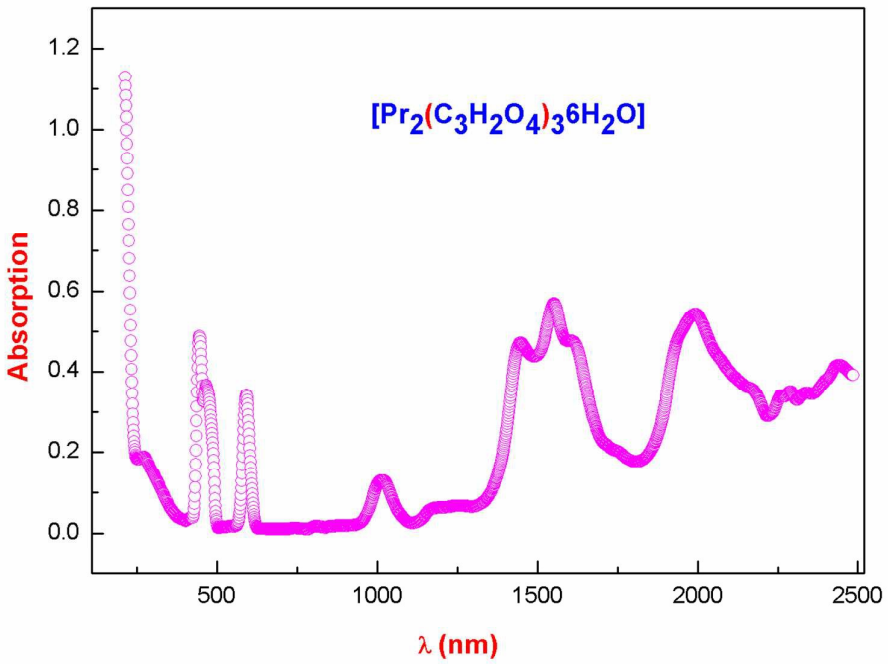

Fig.10. UV-Vis-NIR spectrum of PMH single crystals.

RSC Advances Accepted Manuscript

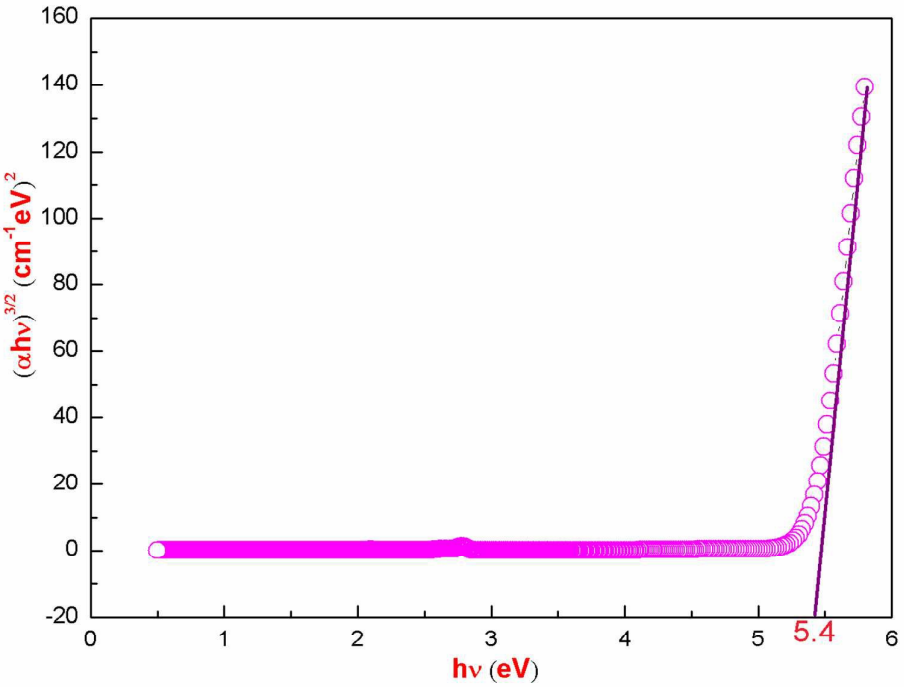

Fig. 11. Touc plot for calculation of the optical band gap of PMH single crystals.

RSC Advances Accepted Manuscript

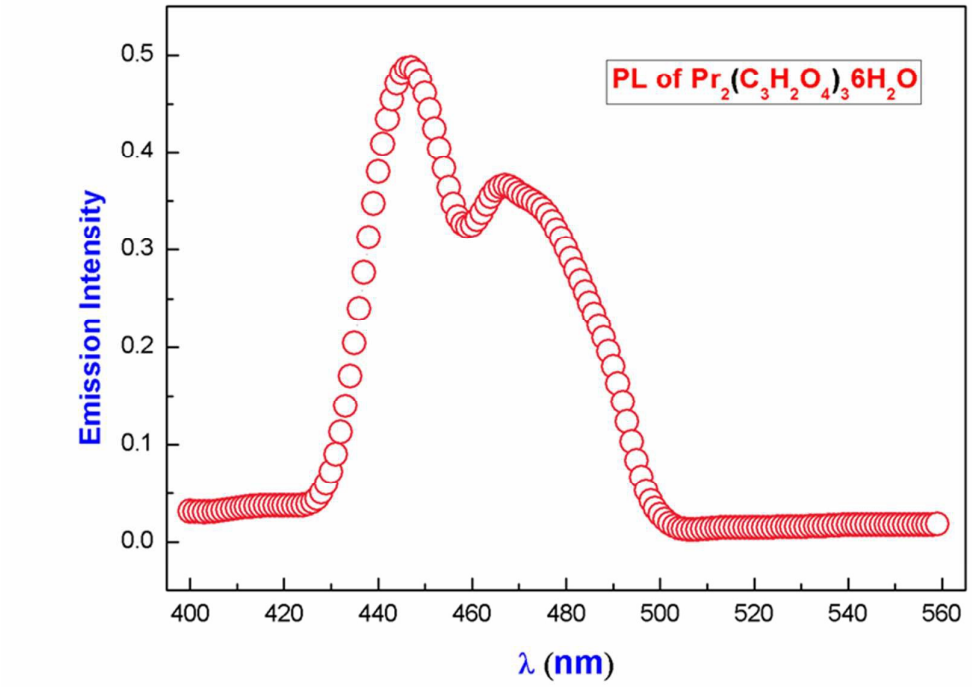

Fig.12. Photoluminescence emission spectra of PMH single crystals.

RSC Advances Accepted Manuscript

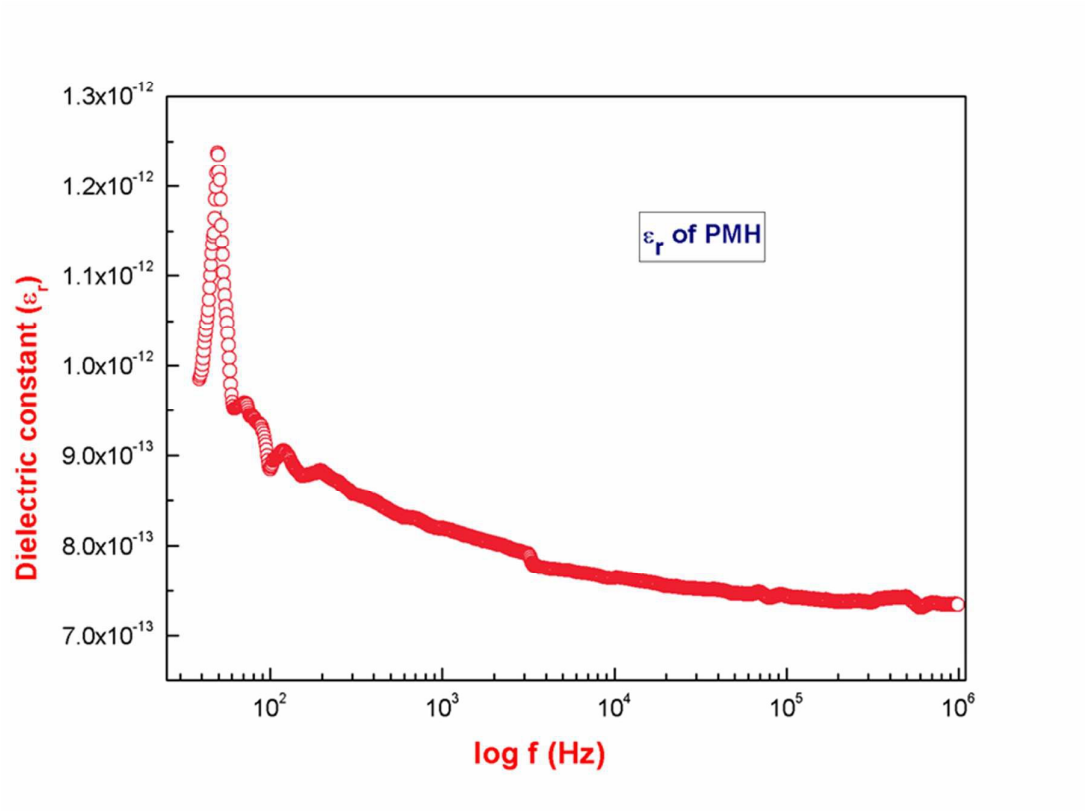

Fig 13. Variation of dielectric constant of $[Pr_2 (C_3H_2O_4)_3(H_2O)_6]$ with frequency of the applied field.

RSC Advances Accepted Manuscript

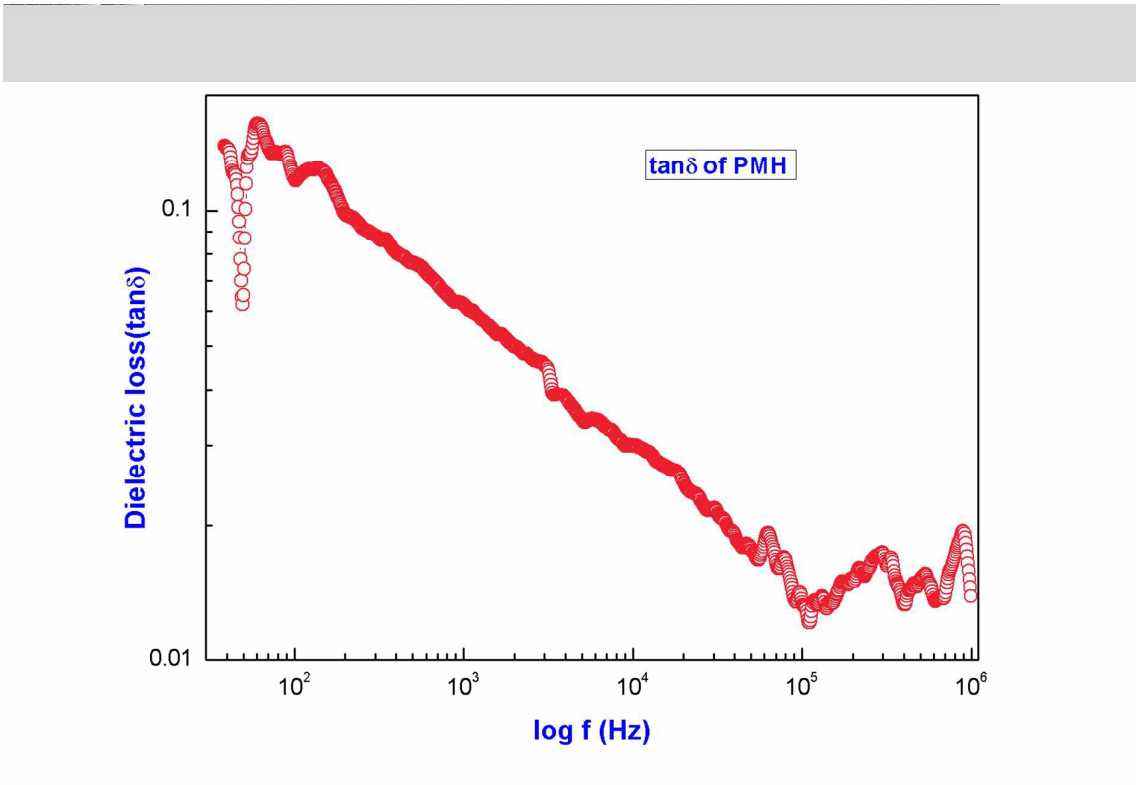

Fig.14. Dependence of dielectric loss on frequency of the applied ac field for $[Pr_2 (C_3H_2O_4)_3 (H_2O)_6]$.

RSC Advances Accepted Manuscript

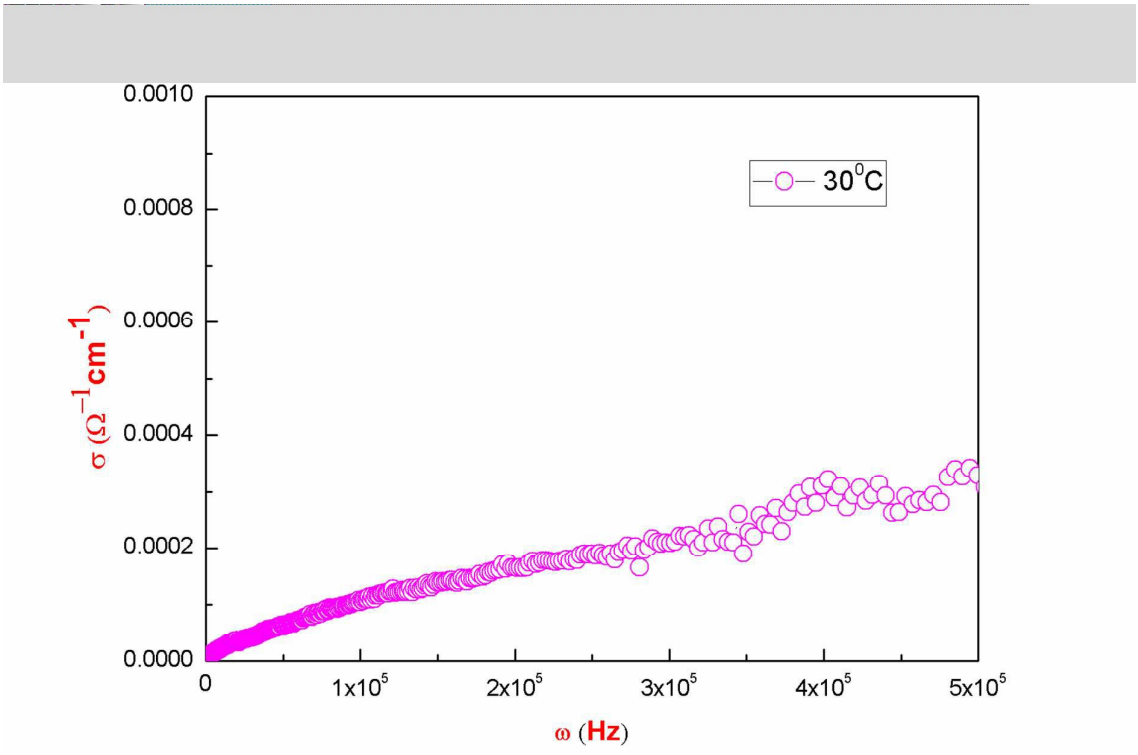

Fig.15. Dependence of conductivity of $[Pr_2 (C_3H_2O_4)_3(H_2O)_6]$ on frequency of the ac field.

RSC Advances Accepted Manuscript

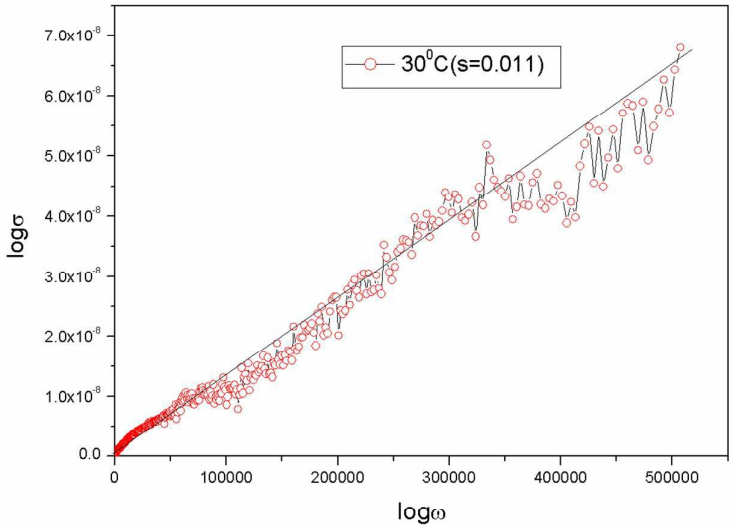

Fig.16. Curve of logσ versus logω.

RSC Advances Accepted Manuscript

Tab. 1 (a).

EDAX analysis of $[Pr_2 (C_3H_2O_4)_3 (H_2O)_6]$ single crystals.

Element	Experimental (%)	Theoretical (%)
Pr	39.844	40.489
Oxygen	42.093	41.375

Tab. 1 (b).

CH analysis of $[Pr_2 (C_3H_2O_4)_3 (H_2O)_6]$ single crystals.

Element	Experimental (%)	Theoretical (%)
Carbon	15.384	15.530
Hydrogen	2.643	2.606

RSC Advances Accepted Manuscript

Tab.2 (a)

Evaluated parameters from powder XRD of PMH crystals.

hkl	2Theta	d (exp)Å	d (cal)Å	intensity	FWHM
-110	10.710	6.25407	5.953	140.0	0.1219
110	13.029	1.08940	0.0003	1397.3	0.0568
-210	14.331	5.10045	4.445	254.6	0.0614
111	16.534	4.35739	3.875	105.4	0.1066
-102	17.495	4.06495	3.649	82.5	0.1161
021	18.314	4.84025	3.485	136.0	0.0762
-212	18.891	4.69384	3.378	100.3	0.0641
400	27.893	3.19610	2.298	77.4	0.1447
122	28.797	3.09774	2.232	85.0	0.0716
-504	37.204	2.01079	1.736	72.1	0.0850
-541	43.203	2.09205	1.501	67.4	0.0550
-534	43.792	2.06056	1.482	69.4	0.0952

RSC Advances Accepted Manuscript

Tab.2 (b).

Crystallite size (L), micro strain (ε), dislocation density (ρ), and distortion parameter (g) calculated from 2 θ values of powder XRD crystals:

2 θ	L (Å)	ε	ρ (in 10^{15}m/m^3)	g
10.710	7.3269	0.0304	18.6	1.446
13.029	15.7244	0.0142	4.0	0.553
14.331	14.5902	0.0153	4.6	0.544
16.534	8.4200	0.0264	14.1	3.394
17.495	7.7391	0.0287	16.7	0.852
18.314	11.8037	0.0188	7.2	0.525
18.891	14.0378	0.0158	5.0	0.429
27.893	6.2986	0.0353	25.2	0.651
28.797	12.7507	0.0175	6.1	0.311
37.204	10.9336	0.0204	8.3	0.284
43.203	17.1814	0.0129	3.4	0.156
43.792	9.9330	0.0224	10.0	0.265

RSC Advances Accepted Manuscript